communications engineering

A Nature Portfolio journal

Article

https://doi.org/10.1038/s44172-026-00656-x

The transonic safe mode as an enabler of next-generation wind turbines

Delphine A. M. De Tavernier ✉, Michiel B. Zaaijer & Dominic A. von Terzi

The wind energy industry is moving towards larger and more powerful turbines, with next-generation designs expected to operate at blade tip speeds exceeding 100 ms^{-1}. These developments introduce new aerodynamic challenges that have not yet been explored. Here we show, using the IEA 22 MW reference turbine as a case study, that large-scale wind turbines may become susceptible to localised transonic flow effects even under normal operating conditions. By analysing the local inflow conditions along the blade and their operational settings, we identify a significant likelihood of transonic flow onset at high wind speeds above 20 ms^{-1} in the outer 10% of the blade span. This is particularly driven by the inherently unsteady nature of wind turbine operation. To address this, we propose and demonstrate a Transonic Safe Mode, a framework designed to limit exposure to transonic conditions. Beyond the specific case study, the paper presents a targeted analysis methodology that highlights the additional investigations proposed to assess and ensure a safe design and operation of large-scale wind turbines. In this context, the Transonic Safe Mode offers a pragmatic and forward-looking pathway for next-generation turbines, enabling proactive risk management while focused research efforts continue to close existing knowledge gaps regarding the impact of transonic flow on wind turbine aerodynamics and structural response.

Wind energy has become an increasingly vital component of the global renewable energy portfolio with advancements in wind turbine technology playing a critical role in meeting the demand for clean and affordable energy[1]. As wind turbine designs evolve the trend points toward larger turbines with longer, more flexible blades and higher tip-speed operation due to system optimisation considerations. The recently introduced IEA 22 MW reference turbine[2] following the IEA 15 MW design[3], exemplifies this trend. With these advancements turbines are now operating under more complex aerodynamic conditions, particularly characterised by high-speed flows at the blade tips. For wind turbines with a rotor radius approaching 140 m the flow velocity at the blade tips exceeds 100 ms^{-1}. These high relative wind speeds introduce a dual aerodynamic challenge: high Reynolds numbers and elevated Mach numbers.

Several researchers amongst them Schepers et al.[4], Brunner et al.[5] and Piqué et al.[6], have recognised the impact of a high (chord-based) Reynolds number, Re, often exceeding 10 million, on airfoil aerodynamics, turbine performance, and loading. While the implications of a higher Mach number (M) have been largely overlooked in wind turbine studies a few exceptions dealt with the onset of compressibility. Sørensen et al.[7] highlighted that for large wind turbines with rotor radii around 100 m blade tips could reach velocities approaching 30% of the speed of sound, suggesting that the assumption of incompressible flow may no longer hold in these regions. Using computational fluid dynamics they explored the effects of compressibility on two-dimensional airfoil aerodynamics and examined the potential for correcting incompressible flow solutions with explicit compressibility corrections. Other researchers amongst them Yan et al. and Archer et al.[8] and those within the EU FP7 AVATAR project[9], have also assessed the influence of compressibility on the performance of large horizontal-axis wind turbines.

In addition to (weak) compressibility effects researchers have studied the effects of transonic and supersonic flow conditions to some extent. Wood et al.[10] investigated how shock-induced stall and the resulting increase in drag, may serve as a natural over-speed protection mechanism for small turbines operating at very high tip-speed ratios. Hossain et al.[11] examined shock propagation on the NREL phase VI wind turbine airfoil at $M = 0.8$. However Sørensen et al.'s[7] work suggests that transonic conditions at these high inflow Mach numbers may not be envisioned during the normal operation of large-scale wind turbines. It was only in 2022 that De Tavernier et al. and Von Terzi et al.[12] demonstrated using standard engineering methods that current and near-future wind turbines are approaching the onset of local supersonic flow around their blades. The inherent unsteady operation of wind turbines was identified to be the driving factor. They demonstrated that the IEA 15 MW wind turbine with a rotor diameter of 242 m and a maximum tip-speed of 95 ms^{-1}, may encounter transonic flow

Flow Physics and Technology, Delft University of Technology, Delft, The Netherlands. ✉e-mail: d.a.m.detavernier@tudelft.nl

conditions during its normal operating regime. While the maximum tip-speed in steady design conditions remains well below the critical Mach number (of the order of M = 0.3) the high (negative) angles of attack encountered by wind turbines cause a significant flow acceleration over the blades. This combination can push the turbine into operational conditions where the Mach number on the airfoil locally exceeds unity. It is particularly pronounced near the cut-out wind speed. Not only are flow velocities higher in these conditions but the blades are also pitched out significantly to maintain the rotor torque. As a consequence the blade encounters angles of attack near −10 to −15 deg close to the tip, leading to large flow acceleration over the airfoil.

For airplanes history has shown that the onset of transonic flow initially caused severe vibrations[13,14] and, in some cases, even structural disintegration (see, for example, the de Havilland DH.108 catastrophic structural failure). Over time the aerospace industry recognised the importance of this flow regime. While the initial strategy focused on avoiding transonic flight conditions later the aviation industry deliberately redesigned airfoils and wings to mitigate these effects, enabling safe and efficient flight in transonic conditions (e.g. Anderson et al.[15,16]). We believe wind turbine technology is approaching a similar stage: turbines are now larger than ever, operate at higher tip-speeds, and are increasingly deployed at scales where transonic phenomena may arise. It is not straightforward to translate learnings from aviation towards wind turbine designs. A key challenge here is that wind turbine airfoils near the blade tip differ substantially from the standard airfoils studied in transonic flow conditions (e.g. Paradiso et al.[17]). Wind turbine profiles are highly cambered and thick and they operate at very high Reynolds numbers. Moreover transonic effects are expected to occur at lower inflow Mach numbers and highly negative angles of attack, a regime that has received almost no experimental nor numerical study. While many studies may only show shocks above Mach 0.5–0.6 for non-wind specific airfoils initial analyses done by Vitulano et al.[18] indicate shock formation at Mach numbers as low as 0.3, driven by the strong leading-edge pressure peaks at turbine-relevant Reynolds numbers.

Pulling an analogy to aviation transonic flow conditions as encountered by wind turbines may introduce aerodynamic consequences that could adversely affect turbine performance and longevity (including shockwave formation, increased drag, and vibrating frequencies caused by transonic buffeting). While we do not claim that transonic flow will inevitably lead to critical issues or failure in wind turbines we emphasise that associated risks cannot currently be ruled out and therefore warrant careful investigation. Instead of focusing solely on potential consequences, it is essential to establish with confidence that operation in this regime does not introduce unacceptable risks. From this perspective when the absence of risk cannot be convincingly demonstrated, a precautionary approach is justified that minimises or avoids potential exposure until safety can be assured.

Therefore this work proposes a pragmatic, forward-looking pathway: it provides a means to proactively manage potential risks while research continues to close knowledge gaps. We propose a technological remedy to mitigate transonic effects on wind turbines, thereby paving the way towards improved turbine design with effective and safe operation outside transonic flow conditions. The transonic safe mode (TSM) similar to the erosion safe mode (e.g. Bech et al.[19]), presents an alternative steady-state operating strategy. Given that the emerging problem of transonic flow is not yet fully established we start by assessing and diagnosing the (potential) occurrence. That analysis builds upon the work described in De Tavernier et al. and Von Terzi et al.[12], but for an increased turbine size representing current wind-turbine market developments, which is expected to be more prone to transonic flow conditions. Subsequently the TSM will be explored for the same turbine.

Results

To elucidate the emergence of transonic flow phenomena in large-scale wind turbines and to evaluate the efficacy of the proposed TSM this work is structured into four complementary parts that progress from fundamental diagnostics to system-level mitigation. We first examine from a fundamental perspective the onset of transonic flow at the airfoil scale, establishing the underlying aerodynamic mechanisms that govern local supersonic flow. We then extend this analysis to the full-turbine configuration identifying how these localised phenomena manifest across the rotor and under which operating conditions they become critical. For this we use the IEA22 MW reference turbine which has a rotor diameter of 284 m, a maximum steady-state tip-speed of 105 ms^{-1}, and an operating regime between 3 and 25 ms^{-1}. Building on these diagnostic insights we introduce the TSM as an operational strategy designed to avoid or alleviate these conditions. Finally we demonstrate its application on the IEA 22 MW reference wind turbine, quantifying its impact on rotor flow topology and operating performance. Together these results provide a coherent progression from understanding the origins of transonic effects to validating a practical framework for their mitigation in next-generation turbine designs. In this study we utilise standard engineering models: the integral boundary-layer method Xfoil for airfoil calculations and the aero-servo-hydro-elastic tool OpenFAST for wind turbine simulations.

Transonic flow at airfoil scale

The onset of transonic flow for a two-dimensional airfoil occurs when the local Mach number (the ratio of flow speed to the speed of sound) approaches unity at any point on the surface. This typically occurs well before the airfoil encounters sonic conditions in terms of its incoming velocity because the surrounding pressure field generates substantial local accelerations, most prominently on the suction side. Through Bernoulli's relation the minimum pressure corresponds to the maximum local flow speed. Consequently locally sonic regions may form even under globally subsonic freestream conditions, and this disparity between local and freestream Mach numbers is the hallmark of transonic onset.

In basic aerodynamic books (see Anderson et al.[20], for example) the so-called critical pressure coefficient $C_{p,cr}$ is expressed as a function of the freestream Mach number M_∞. This expression repeated in Eq. 1 can be derived from the compressible, isentropic Bernoulli equation for a perfect gas, combined with the definition of the pressure coefficient (see the 'Methods' section for the derivation). M_{cr} refers to the conditions under which the flow is defined to be locally critical. For transonic flow the critical Mach number $M_{cr} = 1$, but for safety margin reasons, this variable could also be set to a lower value. γ is the specific heat coefficient and as such, a property of the flow medium. For air γ is typically set to 1.4 for standard conditions. Note that this C_p (lowercase p) differs from C_P (uppercase P) used later in this manuscript for power coefficient.

$$C_{p,cr} = \frac{2}{\gamma M_\infty^2}\left[\left(\frac{1+\frac{1}{2}(\gamma-1)M_\infty^2}{1+\frac{1}{2}(\gamma-1)M_{cr}^2}\right)^{\frac{\gamma}{\gamma-1}} - 1\right] \quad (1)$$

Eq. 1 is useful in many ways but for our purpose, it serves as a means to determine the value of the local C_p needed to achieve a local Mach number M_{cr} for a specific freestream Mach number M_∞. In other words setting M_{cr} to 1 gives the critical pressure coefficient $C_{p,cr}$, i.e. the lowest pressure an airfoil can sustain before sonic flow first appears. In case M_∞ equals 1 no extra flow acceleration is needed and thus $C_{p,cr}$ equals 0. For a freestream Mach number of $M_\infty = 0.5$ the expression states that a local C_p of −1.85 is needed to obtain enough acceleration to fulfil transonic flow conditions. The definition of critical pressure coefficient is visualised in Fig. 1a.

Fig. 1b illustrates the relationship between the pressure coefficient and the inflow velocity for three representative critical Mach numbers as directly implied by Eq. 1. To relate these conditions to an operational parameter Fig. 1c expresses the same constraint in terms of angle of attack α rather than pressure coefficient. This translation is achieved using the following procedure: for each angle of attack the corresponding pressure distribution around the airfoil's surface is obtained (here using Xfoil), and its minimum value (representing the peak local flow velocity) is inserted into Eq. 1 as $C_{p,cr}$ to determine the inflow Mach number at which transonic effects first arise. This yields a mapping between α and the local M_∞ marking the onset of

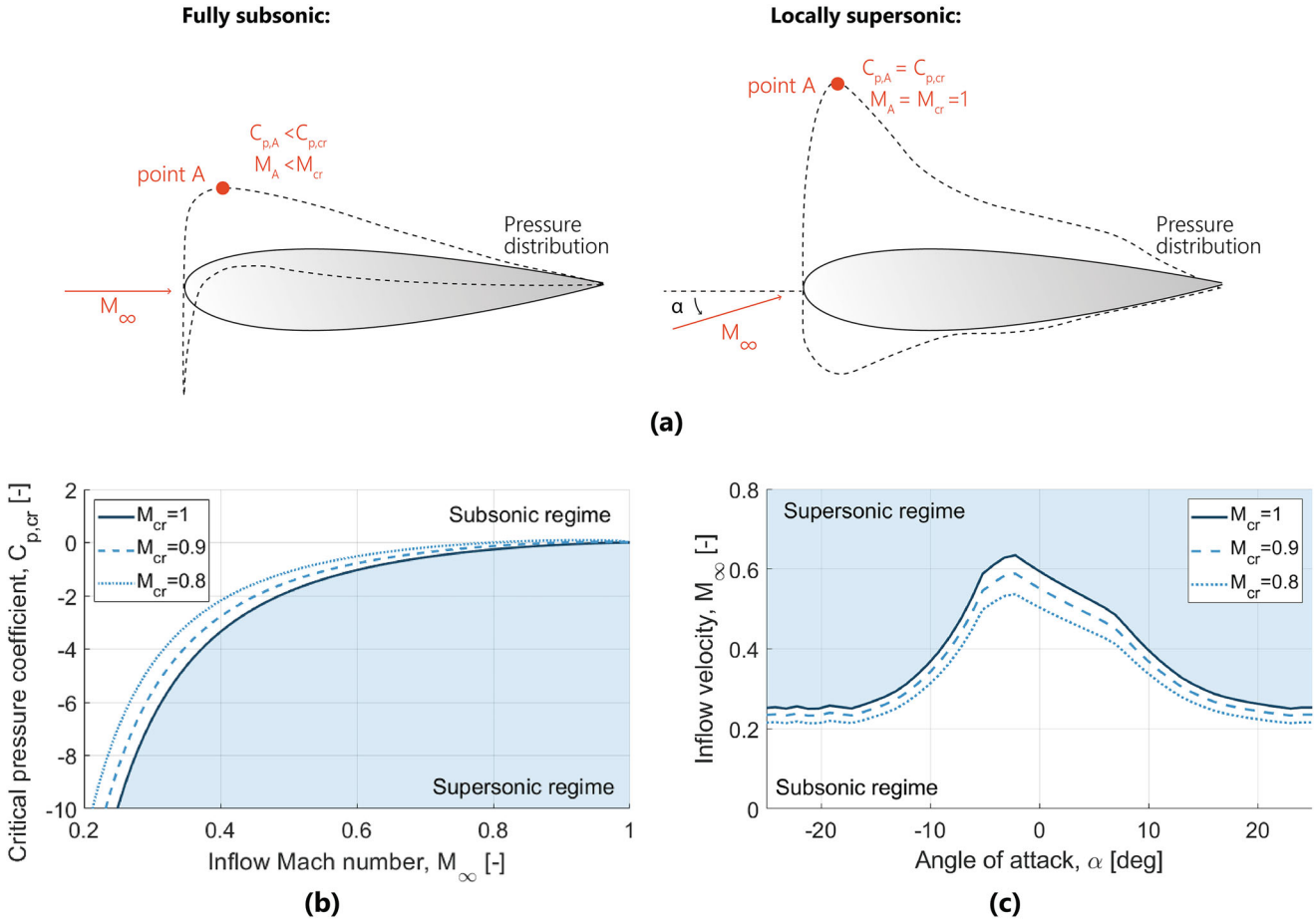

Fig. 1 | Onset of transonic flow on airfoil scale. a Definition of critical pressure coefficient. Point *A* is the location of minimum pressure on the surface of the airfoil at which the local Mach number M_A is reached. **b** Critical pressure coefficient as a function of inflow Mach number for critical Mach numbers M_{cr} = 1, 0.9 and 0.8. **c** The onset boundary of transonic flow as a function of the angle of attack α and inflow velocity M_∞ for which, locally, the critical Mach number is reached. The onset is derived for the FFA-W3-211 airfoil at Re = 1.5×10^7.

transonic flow. The resulting boundary is inherently airfoil-specific depends on the underlying flow characteristics (e.g., Reynolds number and turbulence level), and applies to steady-state conditions. Yet for standard wind turbine (tip) airfoils, it is true that at angles of attack α near zero (or at least the zero-lift angle), the pressure peak is weak, requiring a high inflow velocity for reaching transonic flow conditions. At high angles of attack a relatively high (negative) pressure peak appears, requiring a much slower inflow velocity for transonic onset. For the FFA-W3-211 used in Fig. 1c and at the tip of the blades of the IEA 22 MW reference wind turbine, the flow acceleration over the airfoil surface goes up to four times the inflow velocity, making an inflow Mach number of M_∞ = 0.25 high enough to trigger transonic flow conditions. Despite its simplifications Fig. 1c is expected to be representative of the relevant physics and provides the foundation for this study's framing of transonic onset for wind turbines.

In this work we utilise a simple integral boundary layer method (i.e. Xfoil) to obtain the airfoil's pressure distributions at various angles of attack. This approach has limitations particularly in highly compressible or transonic flow conditions. Yet other studies, both numerically[18] and experimentally[21], have validated and quantified the accuracy of these simulations and have shown that the predictions are within acceptable uncertainty bounds for the (conceptual) purpose of this study. More details on the airfoil simulation set-up are provided in the 'Methods' section.

Transonic flow at turbine scale

As discussed in the previous section the onset of transonic flow over a two-dimensional airfoil section is governed by the interplay between the local angle of attack (through its associated surface-flow acceleration) and the velocity of the incoming freestream. We extend this framework to the three-dimensional wind turbine blade by evaluating the evolving local flow state along the blade span. Wind turbine simulation tools such as OpenFAST provide the time-resolved inflow velocity and angle of attack at each radial station during operation. By superimposing the minimum requirements for the onset of transonic flow onto these locally predicted operating conditions we construct Fig. 2, which maps where and when transonic conditions are expected along the blade. The 'Methods' section details the turbine simulations post-processing steps, and criteria used to generate this figure.

The local inflow conditions are at first glance, set by steady operating conditions, but there is a significant dynamic influence due to wind-speed variations, rotor aerodynamics and blade deflections. The numerically computed outer boundary of the range of conditions is indicated by the shaded area in Fig. 2. While the left figures only demonstrate the extremes of the operating conditions the right figures present the distribution of the time-resolved data. The effects of three parameters are distinguished: (a) wind speed (V_∞), (b) turbulence intensity (TI) and (c) radial position (r/R). Variations are introduced to a baseline case defined as V_∞ = 25 ms^{-1}, TI = 20% and r/R = 98%. The onset of transonic flow M_{cr} = 1.0 is indicated, as well as the onset corresponding to a critical Mach number M_{cr} = 0.9, as a measure for a safety margin.

At V_∞ = 6 ms^{-1}, the IEA 22 MW reference wind turbine experiences a local inflow velocity at the tip near 50 ms^{-1} and an average angle of attack around 10 deg, i.e. close to the design angle of attack of the particular tip airfoil. With increasing wind speed the turbine's rotational speed rises accordingly. Around the so-called rated wind speed i.e. the wind speed

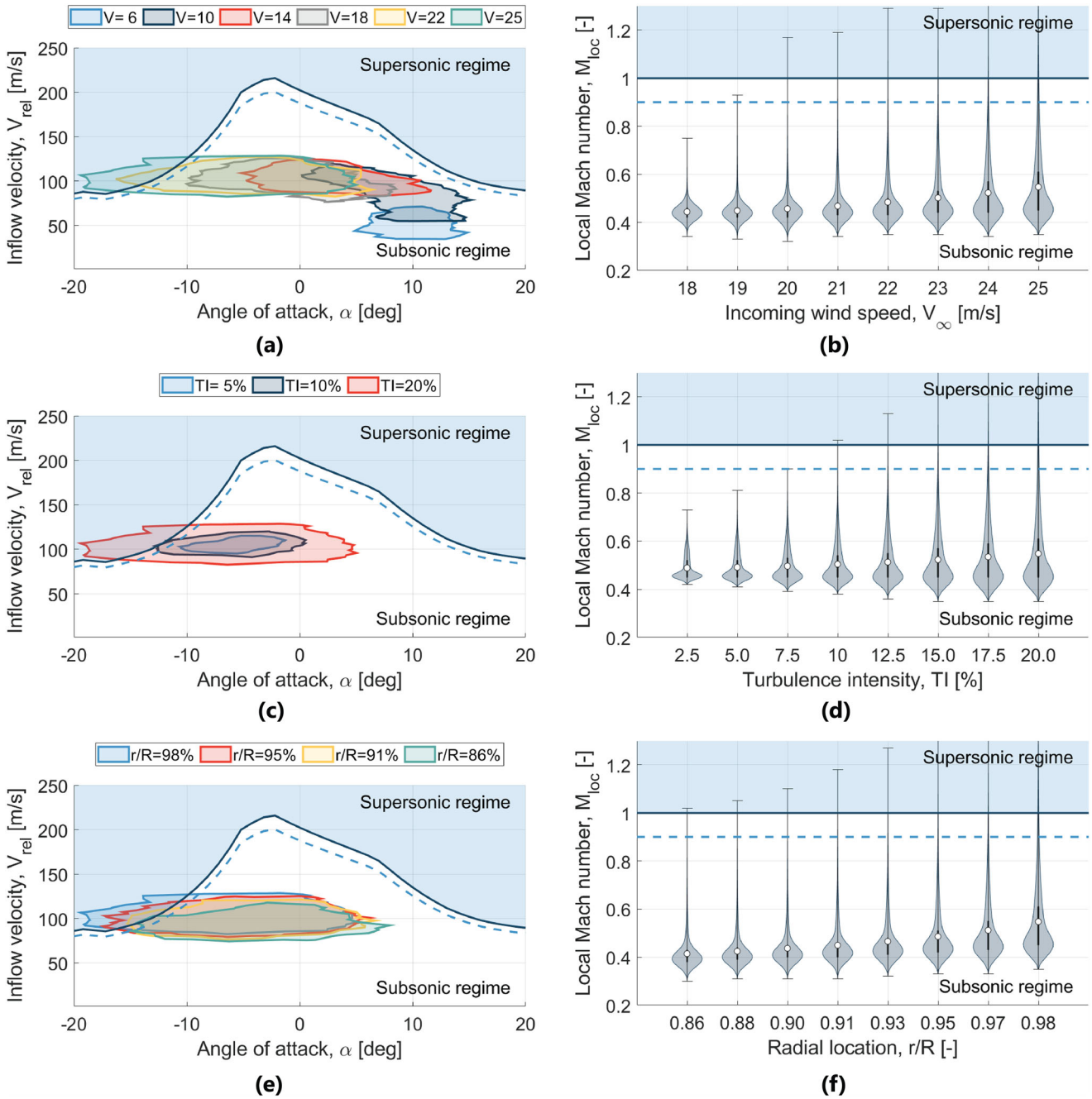

Fig. 2 | The emergence of transonic flow for the IEA 22 MW. Comparison between the local flow conditions of the IEA 22 MW and the transonic onset boundary. On the left the outer boundary of the inflow conditions (specified by angle of attack and relative inflow velocity), obtained within a 1-h simulation. On the right the statistical distribution of the maximum local Mach number in time using a violin box, including the median, 1st and 3rd quartiles. The effect of **a**, **b** incoming wind speed V_∞, **c**, **d** turbulence intensity TI, and **e**, **f** radial location on the blade r/R. Variations are applied to the baseline case: $V_\infty = 25$ ms^{-1}, TI = 20% and $r/R = 98\%$. The transonic onset boundary is indicated for a critical Mach number $M_{cr} = 1$ (solid line) and for $M_{cr} = 0.9$ (dashed line).

where the maximum power output of the wind turbine is attained, the maximum rotational speed is reached. This results in a local inflow velocity approaching the maximum tip-speed of 105 ms^{-1}. This is close to $M = 0.3$ for standard atmospheric conditions at sea level. Starting from the rated wind speed wind turbines pitch out their blades to reduce the torque. This causes the local angle of attack to significantly reduce. Around the cut-out wind speed ($V_\infty = 25$ ms^{-1}) the steady angle of attack close to the blade tip reduces towards nearly −9 deg. This is conceptually visualised in the 'Methods' section using the velocity triangle. Due to the unsteady operational conditions of wind turbines the investigated IEA 22 MW turbine is expected to enter transonic flow conditions for a portion of the time. For the baseline condition (i.e. $V_\infty = 25$ ms^{-1}, TI = 20% and at $r/R = 98\%$) this equals around 2% of the time, which corresponds to 12 s in every 10-min time interval. While the baseline case corresponds to a fairly high TI value it is worth mentioning that in the simulations, no bend-twist coupling of the blade or veer/yawed inflow were considered, nor were any malfunctioning or abnormal operating conditions of the rotor. These aspects can amplify the time at which the turbine is at risk.

Figure 2b indicates the key role of turbulence intensity on the turbine's risk for local supersonic flow. In the absence of any TI or in other words, in steady operating conditions, the turbine is expected to operate well within the safe subsonic regime. However it is the unsteadiness of the flow and the

slow response of the turbine's degrees of freedom that cause a wide spread in the operating area.

Near the blade tip the IEA 22 MW wind turbine is expected to enter transonic flow conditions more frequently, as the outer part of the blades perceives a higher relative velocity and experiences larger variations in angle of attack, due to flapwise motions (see Fig. 2c). The outer 10% of the blade is at risk at cut-out wind speed. For the tip itself (at 98% of the rotor radius) transonic flow conditions are expected from $V_\infty = 20\ \mathrm{ms}^{-1}$ onwards, though for a limited portion of the time only.

Transonic safe mode

At present the operating set-points of large turbines drive blades into transonic conditions. This means that current practices do not guarantee avoidance of this (potentially unsafe) regime and this motivates the introduction of alternative set-points or operational strategies. Therefore we propose the TSM. The TSM itself is any operating condition that avoids transonic flow. However the main purpose of our proposal is to provide a framework in which the turbine can be optimised under the constraint that transonic flow is avoided. This framework introduces new trade-offs between power performance and loading that can affect both rotor design and turbine operation. However instead of prescribing a full optimisation procedure, we provide in this section the underlying methodology for including transonic safe operation in the design, as well as examples to clarify its application. We will examine two illustrative strategies that only adjust operating set-points with distinct additional constraints: one that preserves power output at the cost of increased torque, and another that preserves torque while permitting a reduction in power. The framework will be described first using a power constraint i.e. maintaining power, after which we show that it is applicable in a similar way to torque or other constraints.

In Fig. 3a the so-called C_P iso-lines are indicated for the IEA 22 MW turbine. These iso-lines present a contour map giving the relation between the turbine's tip-speed ratio λ and blade pitch angle β on the one hand and the turbine's (aerodynamic) power coefficient $C_P = P/(\frac{1}{2}\rho V_\infty^3 A)$ on the other hand. C_P is a measure for the aerodynamic efficiency of the blade design and its operation with a value that cannot exceed $16/27 \approx 0.59$, the so-called Betz limit. Note that this C_P (uppercase P) differs from the pressure coefficient C_p (lowercase p) used in Eq. 1. P is the dimensional power, V_∞ refers to the incoming wind speed and A is the wind turbine's frontal area.

As an example the turbine's operation at $V_\infty = 22\ \mathrm{ms}^{-1}$ and TI = 20% is discussed here. At this wind speed the power coefficient needed to reach rated power is only $C_P = 0.058$. In normal operating conditions the turbine aims to operate at a rotational speed of $0.88\ \mathrm{rads}^{-1}$ and a blade pitch angle of 20.84 deg. However in the above-rated region where the power output is fixed at rated, there is freedom in selecting the combination of torque and rotational speed, which is exploited by the proposed operating strategy. Changing the rotational speed will alter the tip-speed ratio (since the wind speed is fixed at $22\ \mathrm{ms}^{-1}$ in this example) which would necessitate an associated change in torque to maintain the power at rated levels. This is achieved by changing the blade pitch-angle. As such multiple combinations of tip-speed ratio and blade pitch provide the same power output. In Fig. 3a these potential combinations, some characterised by a higher rotational speed and others by a lower one, are indicated by the dashed lines. The normal operating mode following its definition from the IEA 22 MW reference turbine's report (see Zahle et al.[2]), is indicated by the marker NM. In Fig. 3b the corresponding local flow conditions near the blade tip are visualised for a few points on the dashed line. The original normal operating mode shows a crossing of the transonic boundary for some time steps. However alternative operating options exist, particularly the ones with a lower tip-speed ratio, that move the operating cloud towards the safe subsonic zone.

Note that no new simulations were conducted. Instead the data are only shifted along the steady-state conditions indicated by the dashed line. To obtain the steady-state inflow velocity and angle of attack from the set-point for tip-speed ratio and blade pitch the induction factor and the section pitch angle need to be known. The induction factor was obtained from the normal steady-state design thrust coefficient. Since the power coefficient is the same for all alternative operating points it can be assumed that the induction factor is also the same at all these points. To determine the angle of attack the section twist angle at the analysed radial position was taken from the IEA turbine report[2]. With this approach it is inherently assumed that the spread of the data is unchanged. This assumption is reasonable for a first approximation as the spread in the operational data is mostly driven by changes in the incoming wind vector (see 'Methods' section). For small adjustments in the operating conditions small-angle approximations are applicable, making this assumption legitimate. For larger adjustments the uncertainties are slightly larger, but for the purpose of this paper, it is well within an acceptable range.

Repeating this approach for every wind speed with risk of transonic flow gives a range of potential operating set-points. In Fig. 4a, b the transonic safe combinations for a TSM preserving power are indicated with the coloured solid lines. The crosses in the same colours correspond to the normal operating points showing that for $V_\infty = 20\ \mathrm{ms}^{-1}$ and above, the normal operating mode falls outside the safe area. While Fig. 4a presents the safe mode as a combination of blade pitch and tip-speed ratio Fig. 4b expresses the safe operating modes in function of blade pitch and rotational speed. These parameters are more intuitive for wind turbine operation and correspond to the turbine's actual degrees of freedom. Here it is no longer possible to add the C_P iso-lines as they become wind speed dependent. Note that in the normal operating mode the rotational speed at wind speeds above rated is typically kept constant.

The previously presented TSM is formulated to maintain power output. As most alternative operating points for a power objective will cause the turbine's torque to increase this strategy is only feasible if sufficient margins exist. This is often not the case for large turbines, where torque is the design driver for the drivetrain. However the concept is not restricted to power-preserving constraints. A complementary TSM could be defined in which torque is prioritised maintaining it at or below a threshold while accepting a reduction in power. In this case the power coefficient (C_P) iso-lines are replaced by the torque coefficient (C_Q) iso-lines. This variant would avoid transonic flow while ensuring structural safety at the cost of some energy capture. The results of this alternative TSM are presented in Fig. 4c, d. In Fig. 4c the iso-lines represent constant torque. Although the lines are harder to distinguish it can still be seen that for $V_\infty = 20\ \mathrm{ms}^{-1}$ and above, the normal operating mode falls outside the safe area.

To operate safely outside the transonic regime whether it is power or torque-driven, the TSM requests both the rotor speed and pitch angle to be adjusted simultaneously in a dependent manner. Both strategies request a reduction in rotational speed but it is the choice in blade pitch angle that sacrifices power and/or torque. We want to convey that there is no unique TSM. Rather a spectrum of possible strategies can be defined, and their selection depends on how designers and operators choose to balance competing objectives. These may include (but are not limited to) thrust, blade bending, tower clearance, limits in minimum/maximum rotational speed and pitch angle, etc. In practice this becomes a multi-objective trade-off where a Pareto front could be constructed, under the constraint of remaining outside the transonic regime. This Pareto front can include various operating strategies but also choices for rotor and drivetrain design variables, for example.

To summarise the analysis of the TSM provides the means for explicitly integrating transonic conditions into the existing optimisation framework of turbine design and operation. The core of the methodology is described by three ingredients that are captured in Fig. 3b. First the boundary between transonic and subsonic flow around an airfoil is captured as a function of the angle of attack and inflow velocity, using the critical pressure coefficient. Second the variable operating conditions for a reference operation are expressed in the same parameters, by time-resolved simulation. Third the variable operating conditions at other set-points are shifted along the line of steady-state operation to identify transonic risk. In addition preliminary

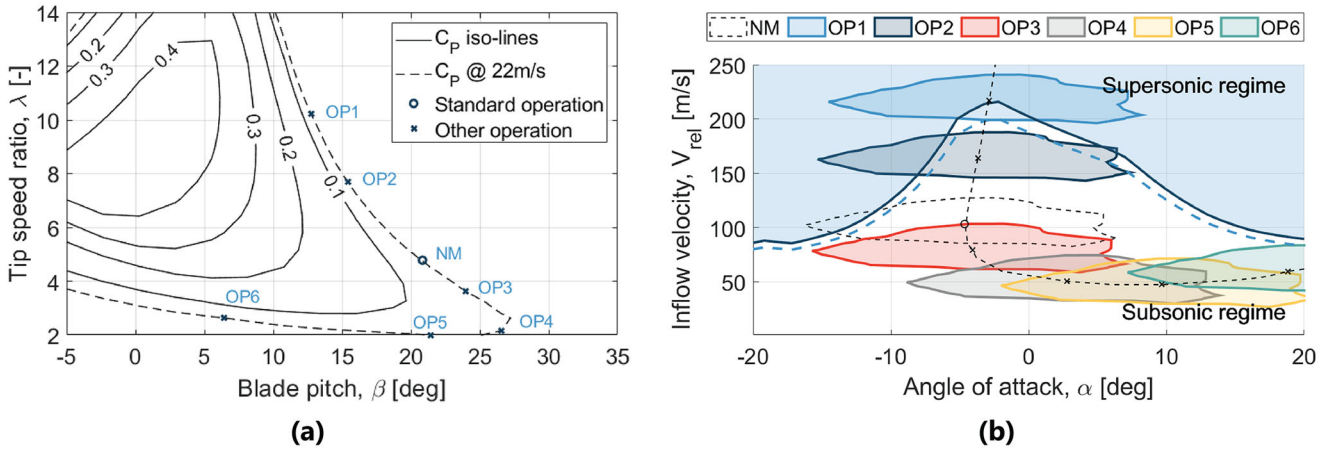

Fig. 3 | Alternative operating conditions with constant power output at $V_\infty = 22\ \mathrm{ms}^{-1}$ at TI = 20%. a Power coefficient iso-lines as a function of tip-speed ratio and blade pitch angle. The dashed iso-line follows the power coefficient needed at $V_\infty = 22\ \mathrm{ms}^{-1}$. Six alternative operating conditions are randomly selected as demonstrations. **b** The local flow conditions at the blade tip ($r/R = 98\%$) during normal operating mode and the six alternative modes. The transonic onset boundary is indicated for a critical Mach number $M_{cr} = 1$ (solid line) and for $M_{cr} = 0.9$ (dashed line). NM: $\lambda = 4.78$, $\beta = 20.84$ deg; OP1: $\lambda = 10.21$, $\beta = 12.76$ deg; OP2: $\lambda = 7.68$, $\beta = 15.41$ deg; OP3: $\lambda = 3.62$, $\beta = 23.95$ deg; OP4: $\lambda = 2.16$, $\beta = 26.58$ deg; OP5: $\lambda = 2.00$, $\beta = 21.45$ deg; OP6: $\lambda = 2.63$, $\beta = 6.46$ deg.

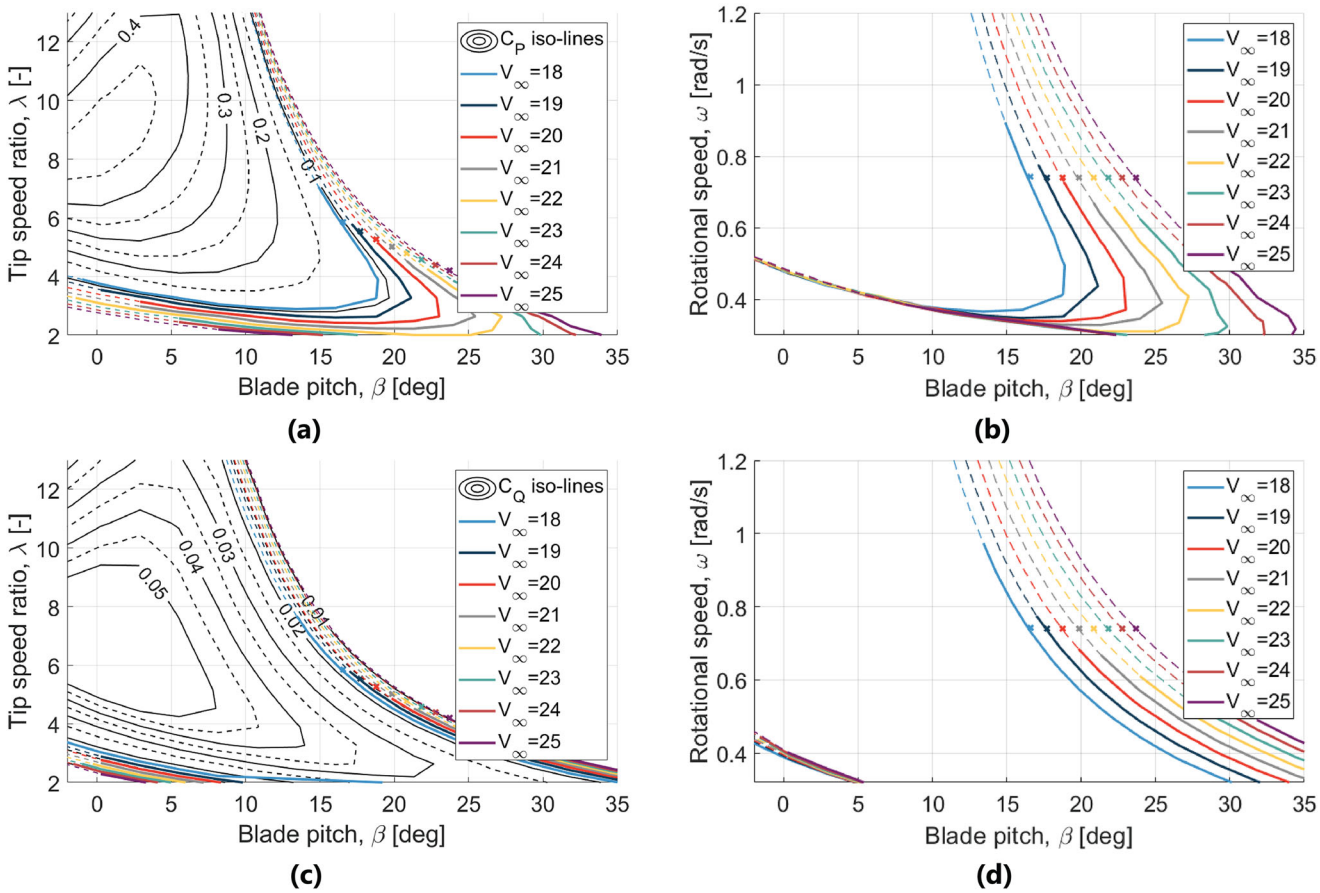

Fig. 4 | Transonic safe alternative modes. a The transonic safe combinations for a constant power coefficient C_P of tip-speed ratio and blade pitch for wind speed from $V_\infty = 18\ \mathrm{ms}^{-1}$ to $V_\infty = 25\ \mathrm{ms}^{-1}$. The iso-lines are indicated in black. **b** The transonic safe combinations for constant C_P expressed in blade pitch and rotor rotational speed. **c** The transonic safe combinations for a constant torque coefficient C_Q of tip-speed ratio and blade pitch for wind speed from $V_\infty = 18\ \mathrm{ms}^{-1}$ to $V_\infty = 25\ \mathrm{ms}^{-1}$. The iso-lines are indicated in black. **d** The transonic safe combinations for constant C_Q expressed in blade pitch and rotor rotational speed. Dashed coloured lines indicate all options with the same power or torque coefficient per wind speed the solid line indicates transonic safe options. The crosses show the normal operating points.

analysis of the effect of constraints on the TSM options can be supported by other perspectives on turbine operation and performance, such as in terms of the power coefficient as a function of tip-speed ratio and blade-pitch angle. The framework can be expanded with improvements in the accuracy of the core ingredients the inclusion of other perspectives to elicit TSM options and the integration of the core ingredients in a numerical optimisation process. A set-point optimiser such as COFLEXOpt[22] could be used for the latter purpose.

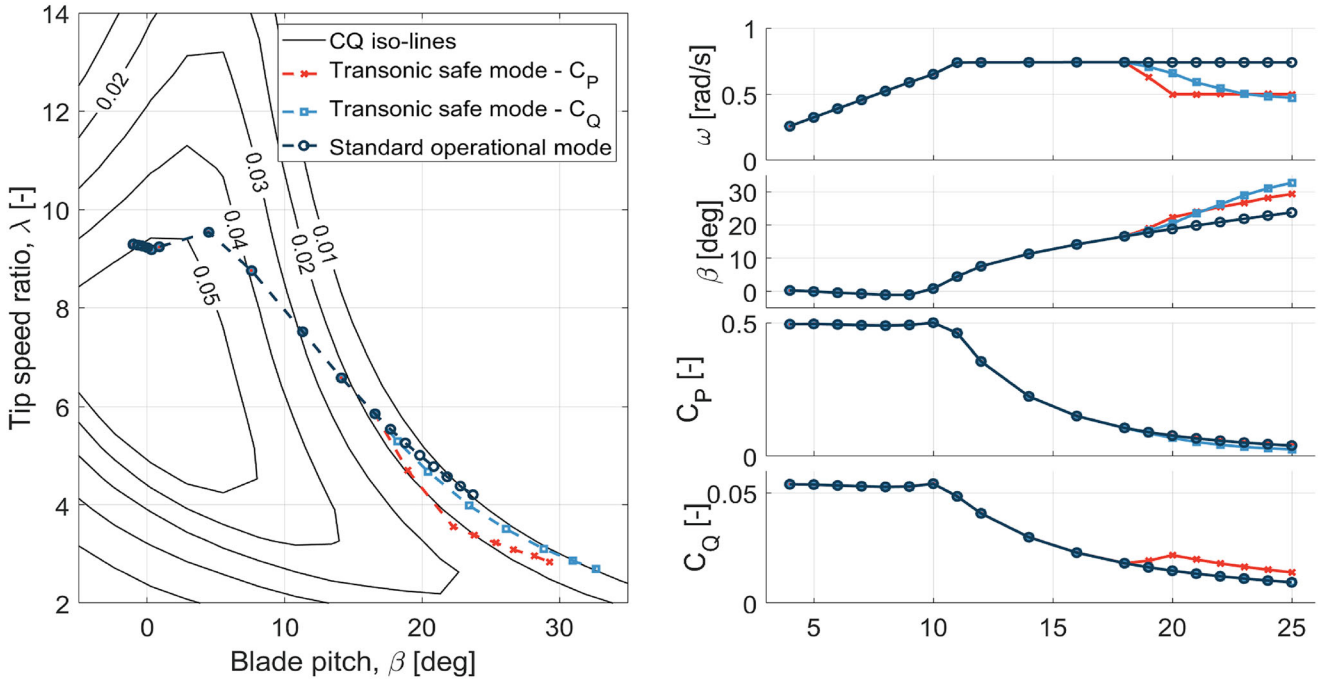

Fig. 5 | Transonic safe mode. A comparison between the standard operational mode of the IEA 22 MW and two alternative modes avoiding transonic flow conditions: one without compromising power output (C_P) and one keeping the torque (C_Q) constant. Note that these modes are not unique but a showcase.

Demonstration of the transonic safe mode. While many transonic safe alternative modes can be identified we will demonstrate two specifically selected safe modes. Both prevent transonic flow from appearing at the turbine's blade tips by applying the methodology from the previous section to all wind speeds to obtain a comprehensive control trajectory. Two (arbitrarily chosen) solutions for two independent isolated constraints are selected: (1) preserving power output and (2) preserving torque, following the descriptions presented in Fig. 4. A transonic safe trajectory is selected as a combination of rotor speeds and pitch angles for each incoming wind speed. It is chosen to only adjust for the wind speeds at risk i.e. above $V_\infty = 20\ \mathrm{ms}^{-1}$, considering a smooth control in response to a change of the wind speed and a reasonable margin to the transonic boundary.

In Fig. 5 the standard operational mode and the TSMs are presented. The chosen TSM preserving power loss opts for a constant rotor speed of $0.5\ \mathrm{rads}^{-1}$ for wind speeds above $V_\infty = 20\ \mathrm{ms}^{-1}$, with a short transitory trajectory. This resembles the standard operating mode closely. The TSM limiting torque opts for a more gradual reduction in the rotational speed from $V_\infty = 18\ \mathrm{ms}^{-1}$ onwards. The blades are in both modes pitched out further (pitch angle is slightly increased).

The turbine's operating conditions are re-evaluated with an adjusted set-point controller. The results are visualised in Fig. 6 where a comparison is made between the standard operating mode and both TSMs. The statistical distribution of the maximum local Mach number at the blade tip is plotted by means of a violin box plot where the minimum and maximum local Mach numbers are indicated with horizontal bounding lines. This plot demonstrates that the TSMs remain well below the transonic onset boundary while this is not the case for the standard operating mode. These examples demonstrate the feasibility of developing a transonic safe operating strategy with multiple constraints.

Discussion

This research paper investigates the emergence of transonic flow conditions in wind turbines that are or have currently been designed (see list of most powerful wind turbines[23]) using the IEA 22 MW reference turbine as a representative example. The study explores the risk of the emergence of transonic flow on large machines by considering the turbine's operating inflow conditions and control settings driving its onset. Using standard engineering methods this manuscript demonstrates, in a diagnostic manner, that the IEA 22 MW reference turbine is expected to encounter transonic flows, particularly under unsteady operational conditions at high wind speeds above $20\ \mathrm{ms}^{-1}$ at the outer 10% of the blade. Although this study uses simplified engineering methods the extent to which the turbine's operating conditions cross the onset of transonic flow is well beyond the uncertainty of the methods employed. To ensure a robust and reliable turbine design this manuscript proposes an alternative analysis and optimisation framework to mitigate these effects by introducing a TSM. This aims to prevent transonic flow under turbine-specific constraints or trade-offs (e.g. for power loss and maximum torque). It is shown how the TSM can be implemented and that it leads to fully subsonic operation of the IEA 22 MW reference turbine.

Although our analysis focuses on the aerodynamic conditions leading to transonic flow it is equally important to recognise why such regimes merit attention from an operational and design standpoint. Experience from high-speed aerodynamics shows that the emergence of local supersonic pockets shocks and associated unsteady phenomena can trigger undesirable load excursions, amplify vibration levels and erode aerodynamic efficiency. Wind turbines are not designed with these regimes as part of their expected operating envelope yet the rapid scaling of rotor diameters and tip-speeds makes occasional excursions increasingly plausible. In this light the central issue is not that transonic effects have already been shown to compromise current turbines, but that their potential impact remains largely uncharacterised. This uncertainty itself represents a risk: safe operation cannot be guaranteed unless the regime is consciously avoided or actively controlled. The framework proposed in this work therefore aims to provide a pragmatic safeguard, limiting exposure to transonic conditions and offering a pathway for future design strategies that maintain performance and safety while reducing reliance on unverified aerodynamic behaviour.

This manuscript is particularly timely given the rapid advancements in wind turbine size. Development of 20+ MW turbines resembling or even exceeding the IEA 22 MW reference turbine has been announced by the industry. Yet the debate on the optimal size of wind turbines is ongoing, with arguments both for and against even larger designs in the future. While the

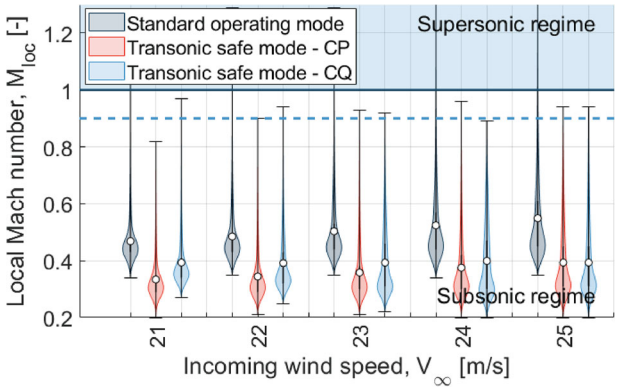

Fig. 6 | Demonstration of transonic safe mode. The statistical distribution of the maximum local Mach number in time by the blade tip ($r/R = 98\%$) presented using a violin box, including the median, 1st and 3rd quartiles. A comparison between standard operational mode and two TSMs (constant power C_P, and constant torque C_Q). The transonic onset boundary is indicated for a critical Mach number $M_{cr} = 1$ (solid line) and for $M_{cr} = 0.9$ (dashed line).

growth in turbine size has massively contributed to the reduction in costs studies show that by considering multi-disciplinary design optimisation and analysis frameworks to minimise LCoE, a global optimum turbine size and rating may be reached. According to Mehta et al.[24] this may likely be (depending on the modelling approach and assumptions) of the order of the IEA 15–22 MW reference turbine, arguing the relevance of the analysis reported here further. While the turbine size per se is not necessarily pushing wind turbines into transonic operating conditions it is the maximum blade tip-speed (generally higher for large turbines due to design trades) and the blade pitching range that make larger turbines more sensitive to transonic flow risks.

Large wind turbines are confronted with a range of important challenges including standstill vibrations, leading-edge erosion and performance uncertainties at high Reynolds numbers, among others. These topics are currently the focus of substantial research efforts which gives confidence that continued progress will enable the realisation of higher tip speeds in future designs. At the same time this positive development is moving turbines closer to the transonic operating regime. Interestingly in-field prototype turbines may not reveal the same issues as their commercial counterparts, as these prototypes are often positioned in lower wind speed areas with low turbulence intensities. This discrepancy emphasises the importance of testing and validating turbine designs under realistic operating conditions to ensure their robustness and reliability in the field.

By addressing this newly identified aerodynamic challenge for wind turbines which may pose a significant threat to turbine designs, we aim to contribute to the development of more resilient wind turbines. We want to emphasise that transonic flow risks for wind turbines should not limit large-scale turbine development, and we call on the community to further develop the understanding of the effect of transonic flow on wind turbine. However focused diagnostic analyses, similar to what was performed in this study, are needed. Considering transonic flow conditions at an early stage and proactively accounting for them in the operation strategy may prevent the need for reactive remedies later in the development process. Operating turbines smartly, using a TSM, could help mitigating transonic risks while considering the trade-off between output power and loads. This safe transition to larger turbines may allow us to enter the age of transonic wind turbines once they are better understood similar to the current state of commercial aviation. The TSM does not only buy time to develop a better understanding of the effect of transonic flow on wind turbines it also allows us to build a generation of large-scale wind turbines with which field experiments on transonic flow can be conducted, while their long-term commercial operation can rely on the safe operation for which they have been designed.

Methods

IEA 22 MW reference wind turbine

The analysis was performed for the IEA 22 MW reference turbine[2]. This upwind three-bladed turbine configuration with variable speed and collective pitch was selected as it mirrors the wind industry's trend of offshore machines. The floating variant installed on a semi-submersible platform connected to a three-line chain catenary mooring system was chosen as the reference. Note that the floating motion only marginally affects the results due to low motion frequencies (see De Tavernier et al. and Von Terzi et al.[12]). The IEA 22 MW turbine has a 142 m rotor radius, a maximum tip-speed of 105 ms^{-1} and operates in a wind regime from 3 to 25 ms^{-1}. The rated wind speed is 11 ms^{-1}. For this rotor design the FFA-W3 airfoil family is used. The IEA 22 MW reference turbine is fully open source. Aero-servo-hydro-elastic input files to model the turbine in HAWC2, HAWCStab2 and OpenFAST are available[25].

Derivation of Eq. 1

This study's framing of transonic flow onset builds on Eq. 1. It determines the critical pressure coefficient $C_{p,cr}$ for a given incoming velocity M_∞. The starting point in deriving this expression is the isentropic relation between static pressure and Mach number for a perfect gas. Let p_∞ and p_A represent the static pressures in the freestream and at point A, respectively:

$$\frac{p_\infty}{p_0} = \left(1 + \frac{\gamma - 1}{2} M_\infty^2\right)^{-\frac{\gamma}{\gamma-1}} \tag{2}$$

$$\frac{p_A}{p_0} = \left(1 + \frac{\gamma - 1}{2} M_A^2\right)^{-\frac{\gamma}{\gamma-1}} \tag{3}$$

For isentropic flow, where the total pressure p_0 is assumed constant, the ratio between the static pressures follows:

$$\frac{p_A}{p_\infty} = \frac{p_A/p_0}{p_\infty/p_0} = \frac{\left(1 + \frac{\gamma-1}{2} M_A^2\right)^{-\frac{\gamma}{\gamma-1}}}{\left(1 + \frac{\gamma-1}{2} M_\infty^2\right)^{-\frac{\gamma}{\gamma-1}}} \tag{4}$$

The pressure coefficient at point A is given by:

$$C_{p,A} = \frac{p_A - p_\infty}{\frac{1}{2}\gamma p_\infty M_\infty^2} = \frac{2}{\gamma M_\infty^2}\left(\frac{p_A}{p_\infty} - 1\right) \tag{5}$$

Combining Eqs. 4 and 5, we have:

$$C_{p,A} = \frac{2}{\gamma M_\infty^2}\left[\left(\frac{1 + \frac{1}{2}(\gamma-1)M_\infty^2}{1 + \frac{1}{2}(\gamma-1)M_A^2}\right)^{\frac{\gamma}{\gamma-1}} - 1\right] \tag{6}$$

Airfoil simulation tool: Xfoil

The integral boundary layer code Xfoil[26] is a viscous-inviscid interaction method designed for predicting airfoil flows and performance. In this framework the flow is decomposed into two regions: the inviscid outer flow where viscosity can be neglected and the thin, viscous shear layer, that is, the inner flow, where the boundary layer plays an important role. The outer flow is solved using a linear-vorticity stream function panel method. The inner flow is described by the integral momentum and kinetic energy equations are consequently combined with a chain of laminar and turbulent closure relations in order to make the problem determinate.

Xfoil was employed in this work to obtain the pressure distribution and thus the pressure peak, along the airfoil surface at a range of angles of attack (from −20 deg to +20 deg). Simulations were performed for the tip airfoil of the IEA 22 MW namely the FFA-W3-221 airfoil, at a Reynolds number of $Re = 1.5 \times 10^7$. Free transition was considered however at these high

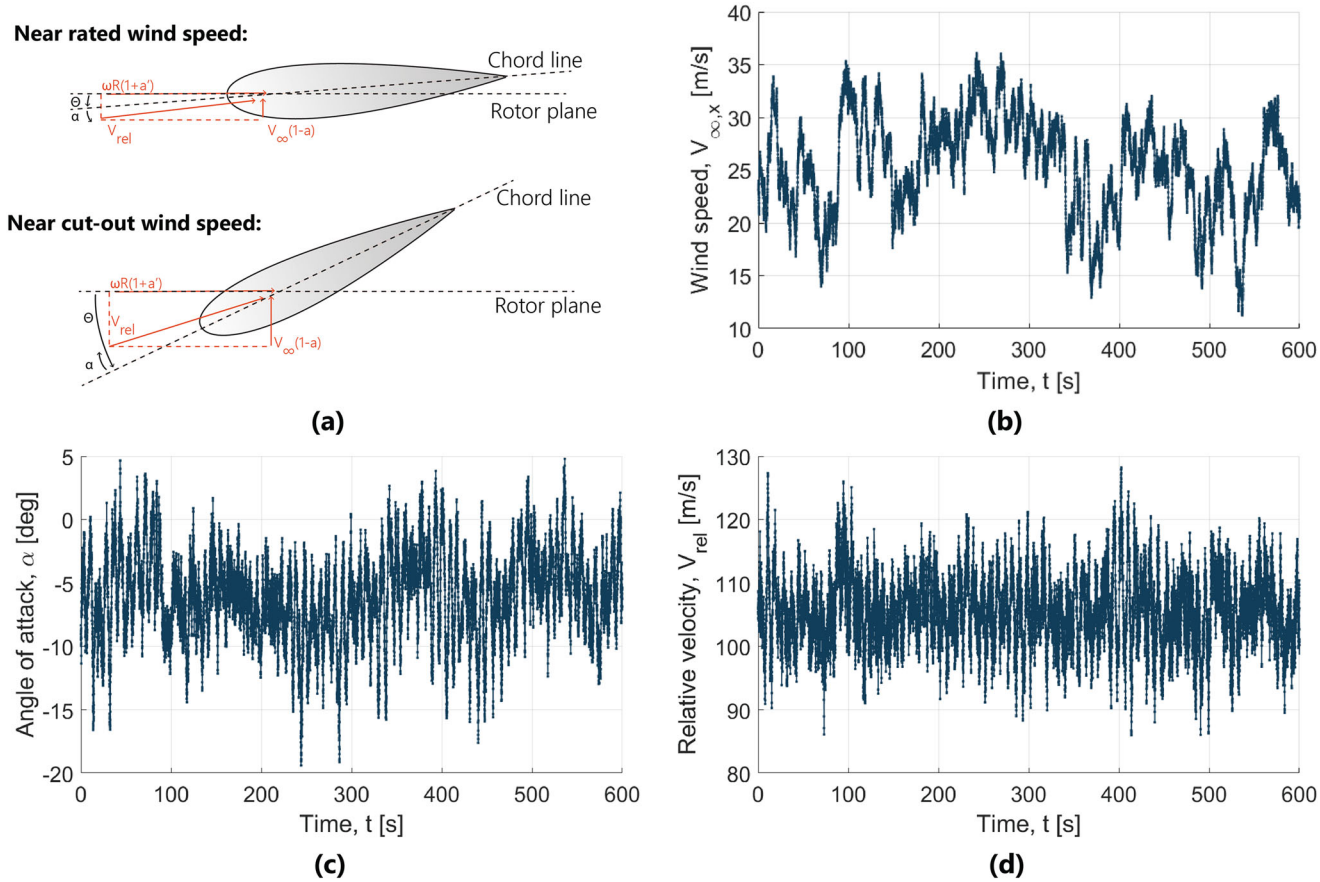

Fig. 7 | Time domain simulation IEA 22 MW. a Graphical illustration of the local inflow properties of an airfoil section near the tip at a near-rated wind speed and cut-out wind speed (Θ is the section pitch angle (the sum of the section twist angle and the blade pitch angle β), α is the angle of attack, a and a' are the axial and radial induction, respectively). **b** Turbulent inflow with a reference wind speed of $V_\infty = 25\ \mathrm{ms}^{-1}$ and turbulence intensity TI = 20%, **c** angle of attack of the blade at 98% radius, **d** relative velocity at the blade at $r/R = 98\%$. Every dot represents a time step.

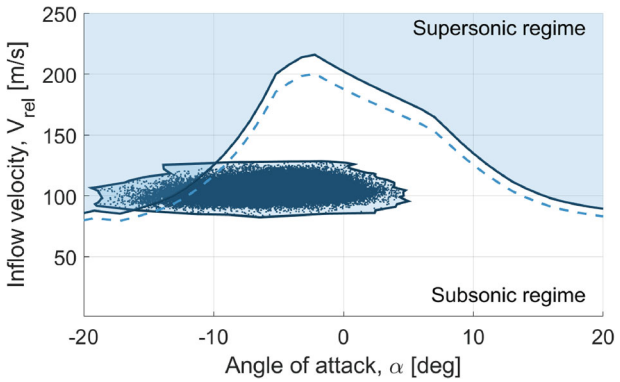

Fig. 8 | Cloud data of operational conditions. Example of how the relative velocity and angle of attack time simulations are restructured into a cloud plot to compare with the transonic onset boundary. $V_\infty = 25\ \mathrm{ms}^{-1}$, TI = 20%. The transonic onset boundary is indicated for a critical Mach number $M_{cr} = 1$ (solid line) and for $M_{cr} = 0.9$ (dashed line).

Reynolds numbers, the natural transition point is expected to be relatively close to the leading edge, arguing that turbulent flow polars would only show marginal differences.

To compensate for compressibility effects the Prandtl–Glauert correction, given by Eq. 7, was applied to convert the incompressible pressure coefficient to the compressible pressure coefficient. The speed of sound c is defined according to the ISA at sea level ($c = 340.3\ \mathrm{ms}^{-1}$). Note that Xfoil is primarily designed for low Reynolds numbers subsonic airfoil analysis, so this correction is just an approximation for mild compressibility effects. It is in fact not suitable for transonic or supersonic flows, where shock waves become significant. Nevertheless the corrected Xfoil is considered accurate enough for this study, as was validated with higher fidelity simulation[18] and experiments[21].

$$C_{p,c} = \frac{C_{p,i}}{\sqrt{1 - M_\infty^2}}, \quad \text{where } M_\infty = \frac{V_\infty}{c} \tag{7}$$

Xfoil is a 2D airfoil modelling tool. However three-dimensional aerodynamic effects are expected to influence the airfoil polars mainly at the blade root and tip. In the inner part of the blades rotational augmentation leads to 3D polar effects. In contrast the outer 5–10% of the blade experiences tip-loss effects that may reduce the effective lift. In the mid-span region however 3D corrections are generally small, and 2D polars provide a sufficiently accurate representation. As the use of 2D polars is common practice in the wind energy community this limitation is assumed to be acceptable for this study.

Turbine simulation tool: OpenFAST and TurbSim

The turbine's operational conditions are evaluated using the open-source software OpenFAST[27]. OpenFAST performs coupled nonlinear aero-hydro-servo-elastic simulation in the time domain.

The OpenFAST simulation performed in this study uses the blade element momentum theory as its aerodynamic model implemented in the AeroDyn module. It uses two-dimensional airfoil lift and drag properties to compute the forces on the blades. AeroDyn accounts for unsteady

aerodynamic effects including dynamic stall and dynamic inflow. The structural module uses a modular multi-body dynamics approach to model the structural behaviour of wind turbines. ElastoDyn is used for low-fidelity structural modelling. It uses a lumped mass approach with the Euler–Bernoulli beam theory and assumes linear structural dynamics from the turbine components. The blade tower and floater degrees of freedom were all enabled.

TurbSim[28] was used to generate a stochastic turbulent wind field with various mean wind speeds. The wind field was defined by a reference wind speed at hub height and a turbulence intensity. The sea state was prescribed by irregular waves identified by the significant wave height and peak period. These parameters were set depending on the reference wind speed, and were defined according to the IEA design standards [IEC 61400-1 (2020), summarised in Allen et al.[29]].

For each mean wind-speed six seeds with an independent wind field were set up. Each seed covers a time span of 10 min. The first few seconds were disregarded to avoid the transient behaviour in the analysis. The simulation time step was set to 0.01 s.

From time domain data to cloud plots

OpenFAST allows the simulation of the angle of attack and relative velocity along the blade for a given input wind speed and sea state. In Fig. 7c, d the local operating conditions at the blade tip are visualised for a mean inflow velocity near cut-out at $V_\infty = 25\ \mathrm{ms}^{-1}$. The turbulent wind profile at hub height is presented in Fig 7b. Every distinct timestep considered in the simulation is indicated with a marker.

Combining this information allows for generating the cloud plot shown in Fig. 8 where the angle of attack seen by the blade at every time instant is plotted versus the relative velocity experienced by the blade (here at $r/R = 98\%$). The outer contour of the operating conditions is emphasised. The shaded blue area indicates the transonic regime as explained in Fig. 1.

Data availability

The data that support the findings of this study are available on 4TU.ResearchData with the identifier data https://doi.org/10.4121/9fce63f7-a5b7-4d72-97a7-90a858098ee2.

Received: 29 April 2025; Accepted: 18 March 2026;
Published online: 02 April 2026

References

1. Veers, P. et al. Grand challenges in the science of wind energy. *Science* **366**, eaau2027 (2019).
2. Zahle, F. et al. *Definition of the IEA Wind 22-megawatt Offshore Reference Wind Turbine*. Report E-0243 (DTU Wind Energy, 2024).
3. Gaertner, E. et al. *Definition of the IEA Wind 15-megawatt Offshore Reference Wind Turbine*. Report NREL/TP-5000-75698 (National Renewable Energy Laboratory, 2020).
4. Schepers, G. *Project Final Report: Advanced Aerodynamic Modelling, Design and Testing for Large Rotor Blades* Report (EERA, AVATAR, 2017).
5. Brunner, C. E., Kiefer, J., Hansen, M. O. L. & Hultmark, M. Study of Reynolds number effects on the aerodynamics of a moderately thick airfoil using a high-pressure wind tunnel. *Exp. Fluids* **62**, 178 (2021).
6. Piqué, A., Miller, M. A. & Hultmark, M. Characterization of the wake behind a horizontal-axis wind turbine (HAWT) at very high Reynolds numbers. *J. Phys. Conf. Ser.* **1618**, 062039 (2020).
7. Sørensen, N. N., Bertagnolio, F., Jost, E. & Lutz, T. Aerodynamic effects of compressibility for wind turbines at high tip speeds. *J. Phys. Conf. Ser.* **1037**, 022003 (2018).
8. Yan, C. & Archer, C. Assessing compressibility effects on the performance of large horizontal-axis wind turbines. *Appl. Energy* **212**, 33–45 (2018).
9. Sørensen, N. N. et al. *Engineering Models for Complex Inflow Situations*. Report 2.8 (AVATAR project, 2017).
10. Wood, D. Some effect of compressibility on small horizontal-axis wind turbines. *Renew. Energy* **10**, 11–17 (1997).
11. Hossain, M. A., Huque, Z. & Kammalapati, R. R. Propagation of shock on NREL phase VI wind turbine airfoil under compressible flow. *J. Renew. Energy* **2013**, 653103 (2013).
12. De Tavernier, D. & Von Terzi, D. The emergence of supersonic flow on wind turbines. *J. Phys. Conf. Series* **2265**, 042068 (2022).
13. Lagemann, E., Brunton, S., Schröder, W. & Lagemann, C. Towards extending the aircraft flight envelope by mitigating transonic airfoil buffet. *Nat. Commun.* **15**, 5020 (2024).
14. Talay, T. *Introduction to the Aerodynamics of Flight, Chapter 5: Transonic Flow*. Report NASA SP-367 (NASA History Division, Langley Research Center, 1975).
15. Anderson, J. History of high-speed flight and its technical development. *AIAA J.* **39**, 761–771 (2001).
16. Anderson, J. *Research in Supersonic Flight and the Breaking of the Sound Barrier* (The NASA History Series, 2001).
17. Paradiso, N. *Investigation at High and Low Subsonic Mach Numbers of Two Symmetrical 6-percent-Thick Airfoil Sections Designed to have High Maximum Lift Coefficients at Low Speeds*. Report (National Advisory Committee for Aeronautics, 1952).
18. Vitulano, M., De Tavernier, D., De Stefano, G. & von Terzi, D. Numerical analysis of transonic flow over the FFA-W3-211 wind turbine tip airfoil. *Wind Energy Sci.* **10**, 103–116 (2025).
19. Bech, J., Hasager, C. & Bak, C. Extending the life of wind turbine blade leading edges by reducing the tip speed during extreme precipitation events. *Wind Energy Sci.* **3**, 729–748 (2018).
20. Anderson, J. D. J. *Fundamentals of Aerodynamics*, 5th edn (McGraw-Hill, 2001).
21. Aditya, A., De Tavernier, D., Schrijer, F., van Oudheusden, B. & von Terzi, D. Experimental study of transonic flow over a wind turbine airfoil. *Wind Energy Sci.* **10**, 2925–2946 (2025).
22. Lazzerini, G. et al. COFLEX: a novel set point optimiser and feedforward-feedback control scheme for large, flexible wind turbines. *Wind Energy Sci.* **10**, 1303–1327 (2025).
23. List of most powerful wind turbines https://en.wikipedia.org/wiki/List_of_most_powerful_wind_turbines Accessed on 2026-Mar-17.
24. Mehta, M., Zaaijer, M. & von Terzi, D. Drivers for optimum sizing of wind turbines for offshore wind farms. *Wind Energy Sci.* **9**, 141–163 (2024).
25. Zahle, F. et al. IEAWindTask37/IEA-22-280-RWT: v1.0.1 https://doi.org/10.5281/zenodo.10944127 *Zenodo* (2024).
26. Drela, M. Xfoil: an analysis and design system for low Reynolds number airfoils. in *Low Reynolds Number Aerodynamics* (Springer-Verlag, 1989).
27. National Renewable Energy Laboratory. Openfast v3.5.3 Online; Accessed on 26-Feb-2025 https://github.com/openfast/openfast/ (2024).
28. National Renewable Energy Laboratory. Turbsim v1.5.0 Online; Accessed on 29-Jul-2021 https://www.nrel.gov/wind/nwtc/turbsim.html (2009).
29. Allen, C. et al. *Definition of the UMaine VolturnUS-S Reference Platform Developed for the IEA Wind 15-megawatt Offshore Reference Wind Turbine*. Report NREL/TP-5000-76773 (National Renewable Energy Laboratory, 2020).

Acknowledgements

The authors would like to acknowledge Bas Verschoor for the support in articulating the working principles and novelties of the transonic safe mode.

Author contributions

All authors contributed to the conceptualisation of the study. D.D.T., M.Z. and D.v.T. developed the methods and approach, while D.D.T. performed the simulations. D.D.T. led the writing of the initial draft, with feedback and improvements from M.Z., D.v.T.

Competing interests
The authors declare no competing interests.

Additional information
Supplementary information The online version contains Supplementary material available at https://doi.org/10.1038/s44172-026-00656-x.

Correspondence and requests for materials should be addressed to Delphine A. M. De Tavernier.

Peer review information *Communications Engineering* thanks the anonymous reviewers for their contribution to the peer review of this work. Primary handling editors: [Rosamund Daw]. A peer review file is available.